Structure and Dynamics of Perfluoroalkane/β-Cyclodextrin Inclusion Compounds As Studied by Solid-State ^{19}F MAS and ^{1}H →^{19}F CP/MAS NMR Spectroscopy

Hiroto Tatsuno and Shinji Ando*

Department of Organic and Polymeric Materials, Tokyo Institute of Technology, Ookayama, Meguro-ku, Tokyo 152-8552, Japan

Received: July 19, 2006; In Final Form: October 14, 2006

The molecular structure and dynamics of novel inclusion compounds (ICs) consisting of *n*-perfluoroalkane (PFA) guests and β-cyclodextrin (β-CD) host (PFA/β-CD) have been investigated using ^{19}F magic angle spinning (MAS) and ^{1}H→^{19}F cross polarization (CP)/MAS NMR spectroscopy with the aid of thermal analyses, FT−IR spectroscopy, and X-ray diffraction method. The ICs of C_9F_{20}/β-CD and $C_{20}F_{42}$/β-CD were successfully obtained as precipitates from mixtures of respective PFAs and saturated aqueous solution of β-CD. The wide-angle X-ray diffraction (WAXD) revealed that C_9F_{20}/β-CD forms a channel-type crystallite, while $C_{20}F_{42}$/β-CD is nearly amorphous at room temperature. The structural orders in both ICs increase at elevated temperatures. The ^{19}F NMR signals obtained by the direct polarization (DP) method for PFA/β-CD are resonated at higher frequencies than those for original PFA. This can be ascribed to the lower dielectric environment of the β-CD cavity. Above 80 °C, ^{1}H→^{19}F CP/MAS NMR technique revealed that C_9F_{20} molecules undergo vigorous molecular motion and partly come out of the β-CD channel. However, the guests hardly degrade or evaporate unless the host is pyrolytically decomposed above ca. 300 °C. The spin-lattice relaxation times in the laboratory frame for ^{19}F (T_1^F) are almost identical for all the fluorines in PFA/β-CD at each temperature, while significantly different values were observed for fluorines in neat PFA. This indicates that effective intramolecular spin diffusion occurs within a PFA molecule included in β-CD.

Introduction

Perfluoropolymers such as poly(tetrafluoroethylene) (PTFE), poly(perfluoroalkoxyethylene)s, and poly(trifluoromethyl-substituted perfluorodioxole)s are known as high performance and functional materials that exhibit a variety of outstanding properties: thermal stability, chemical resistance, low surface tension, low coefficient of friction, low dielectric constant, and low refractive index.[1] Despite such invaluable advantages, applications of perfluoropolymers to blends or composites are less advanced due to their incompatibility with unfluorinated materials. Hence, technologies for producing composites or hybrids to overcome the disadvantages of perfluoropolymers require an innovative strategy. As an effective and facile approach, we focused on cyclodextrin (CD) as an inclusion host. CDs are cyclic oligosaccharides consisting of several D-glucopyranose units. The α-, β-, and γ-CD, which possess six, seven, and eight glucopyranose units respectively, are widely used in various scientific fields because of their versatile capability to include not only small molecules but also polymers in their hydrophobic cavities.[2−4] Actually, there has been numerous studies on CD inclusion compounds (ICs) using various polymers or oligomers as guest compounds: water-soluble linear polymers like poly(ethylene oxide),[5−8] water-insoluble linear polymers such as polyesters and poly(dimethylsiloxane),[9−21] linear oligomers,[22−24] and hyperbranched polymers.[25] Most of the polymer/CD ICs form 'channel-type' structures in which an extended polymer chain threads the tunnel-like cavity of stacked CDs like a string through beads.[4]

In contrast, to our best knowledge, CD ICs consisting of perfluorinated compounds have not been studied except for a work that reported perfluorinated polyethers/CD ICs.[26] Some reports have mentioned that fluorocarbon-modified polymers[27] or fluorinated surfactants[28] can form ICs efficiently with β-CD in aqueous solution. There is also an indication that semifluorinated alkanes[29] or perfluoroalkanes (PFAs)[30] are more likely to be included by β-CD than α-CD, resulting in precipitates. We anticipated that β-CD can form inclusion compounds with PFAs, though the formation of ICs and the structures in the solid state for these compounds have never been investigated. A possible driving force for the inclusion is hydrophobic interaction. The inside of the β-CD cavity is known to be more hydrophobic, in other words, less polarizable or lower dielectric, than the outside because all the hydroxyl groups in a β-CD molecule point toward the outside. PFA may crawl into a hydrophobic cavity to avoid contact with water molecules. If PFAs and β-CD actually can form solid-state ICs, they may occupy an important place in the implementation of novel fluorine-containing materials. For instance, PFA/β-CD ICs are expected to be more compatible with unfluorinated materials than bulk PFAs because all the fluorine atoms of PFA are covered with β-CD molecules. In fact, there have been several studies on polymer blends that are inherently immiscible through covering individual chains with CDs.[12,19] PFA/β-CD IC also has another important implication. Studies on single isolated polymer chains are one of the most fundamental subjects in polymer science. In the case of perfluoropolymers, it is generally difficult to collect information about isolated chains because of their insolubility against common solvents and high melting viscosity. In contrast, a single PFA molecule in the β-CD channel can virtually be considered as an isolated chain in the

* Corresponding author. Tel: +81-3-5734-2137. Fax: +81-3-5734-2889. E-mail: sando@polymer.titech.ac.jp.

10.1021/jp064579k CCC: $33.50
Published on Web 11/23/2006

sense that no PFA molecules are adjacent to each other. Therefore, it is not only for technological but also for fundamental interest to investigate the molecular structures and dynamics of PFA/β-CD ICs.

Solid-state NMR is one of the most powerful tools to investigate both molecular structure and dynamics of solid-state CD ICs in detail for both cases in which guest compounds are small molecules[31−34] and polymers.[8−13] Tonelli and co-workers have been reported the dynamics of both CDs and guest polymers using ^{1}H→^{13}C cross polarization (CP)/magic angle spinning (MAS) NMR,[9−12] and other studies utilize it to characterize insoluble ICs. Recently, static ^{2}H NMR and ^{1}H MAS NMR have been also used for the analyses of dynamics.[8,13] In contrast, solid-state ^{19}F NMR should also be applicable and useful to investigated the PFA/β-CD ICs since PFAs contain many fluorines. Due to the 100% of natural abundance and the wide chemical shift range of ^{19}F nuclei, ^{19}F NMR allows detailed analysis of the chemical structures, conformations, and molecular mobility of fluorine-containing materials, which can be complimentary to the ^{13}C CP/MAS NMR analysis. Moreover, ^{1}H→^{19}F CP/MAS NMR possesses a potential advantage for the analysis of phase structures and molecular dynamics of the materials containing both fluorine and hydrogen atoms in their systems.[35−40] The CP technique is widely used to enhance the signal intensity of rare spins like ^{13}C, and it is utilized for analysis of molecular mobility and estimation of internuclear distances between abundant and rare spins. Although ^{1}H→^{19}F CP/MAS technique does not improve the signal-to-noise ratio because both ^{1}H and ^{19}F are abundant spins, this technique preferentially provides information on fluorines closely located to hydrogens with restricted motion. In the case of PFA/β-CD ICs, the ^{1}H→^{19}F CP/MAS signals can validate the proximity of PFA and β-CD on the molecular level because PFAs possess no hydrogen atoms and β-CD contain no fluorines.

In this paper, we investigated the molecular structure and dynamics of PFAs in β-CD ICs using ^{19}F MAS and ^{1}H→^{19}F CP/MAS NMR spectroscopy with the aid of thermal analyses, infrared spectroscopy, and X-ray diffraction method.

Experimental Section

Materials. *n*-Perfluorononane (*n*-C_9F_{20}) was purchased from Tokyo Kasei Kogyo Co., Ltd. and used without further purification. *n*-Perfluoroeicosane (*n*-$C_{20}F_{42}$) was purchased from Lancaster and recrystallized from a fluorinated solvent before use. β-CD was purchased from Wako Pure Chemical Industries, Ltd. and recrystallized from distilled water. C_9F_{20}/β-CD inclusion compound (IC) was prepared by the following scheme. *n*-C_9F_{20} (0.2 mmol) and a saturated aqueous solution of β-CD (40 mL) were mixed and vigorously stirred for 72 h at room temperature, which yielded a white precipitate. The obtained precipitate was filtered and washed with water to remove free CDs, followed by drying under vacuum at room temperature to remove uncomplexed C_9F_{20}. $C_{20}F_{42}$/β-CD IC was prepared as follows. *n*-$C_{20}F_{42}$ (0.2 mmol) was dissolved by heating in Fluorinert (30 mL, Sumitomo-3M Limited). Fluorinert is a family of perfluorinated liquids exhibiting unique properties such as inertness, insulation, fluidity, and flame retardancy. β-CD aqueous solution (50 mL) was then added and stirred for 72 h at ambient temperature, which yielded white cloudy solution. White flocculation was gradually generated between the aqueous and fluorous layers in the solution. The fluorous layer was removed and the flocculation was centrifuged before drying under vacuum to remove residual solvent. The obtained product looks flaky, showing a different texture from that of C_9F_{20}/β-CD IC.

Nuclear Magnetic Resonance. Solid-state ^{19}F NMR experiments were performed on a JEOL EX spectrometer operating at resonance frequencies of 282.65 MHz for fluorine and 300.40 MHz for proton with a Chemagnetics APEX ^{19}F/^{1}H dual-tune probe and 4 mm o.d. zirconia Pencil rotors. Samples were spun at the magic angle at a rate of $\omega_r = 15$ kHz. The magic angle was adjusted by monitoring the ^{19}F signal of α,α,α-trifluorotoluene included in *p-tert*-butylcalix[4]arene.[42] The temperature inside the rotor was calibrated using ^{1}H chemical shifts of ethylene glycol adsorbed on tetrakis(trimethylsilyl)silane spun at the same rate (15 kHz).[43] The temperatures were precisely controlled between −40 and 120 °C. Fluorine chemical shifts are referenced to hexafluorobenzene, which is assigned a value of −163.6 ppm with respect to $CFCl_3$ with 85 kHz of proton decoupling field to correct the Bloch−Siegert effect.[44] All the samples except neat C_9F_{20} were packed at the center of the rotor with 3 mm thickness along the axis direction to ensure homogeneity of the rf field and temperature. Since neat C_9F_{20} is liquid at room temperature, it was absorbed in cotton batting, which was packed in above-mentioned way.

For all the experiments, the fluorine $\pi/2$ pulse width was set to 2.5 μs, and the fluorine spin-lock field was 100 kHz. ^{19}F DP measurements for CD ICs required a short spin locking (up to 1 ms) before data acquisition to suppress the background signal because CD ICs are less sensitive than neat PFA due to their lower volume fractions of fluorine. The inherent signal intensities were not reduced by the short spin locking because the spin-lattice relaxation times in the rotating frame for fluorine ($T_{1\rho}^F$) are much longer than 20 ms for all the samples. The spin-lattice relaxation times in the laboratory frame for fluorine (T_1^F) were measured by the inversion recovery technique. The recovery time was varied from 0.01 to 20 s. In ^{1}H→^{19}F CP/MAS experiments, the fluorine and proton spin-lock frequencies were adjusted to fulfill the Hartmann−Hahn sideband matching condition, $\omega_{1H} = \omega_{1F} - \omega_r = 85$ kHz. Since ^{19}F signal intensity oscillates as a function of contact time,[36−39] we obtained a variation in intensity in advance and fixed the contact times as 0.1 ms for C_9F_{20}/β-CD and 0.2 ms for $C_{20}F_{42}$/β-CD at which the magnetization transfer occurs most effectively.

Other Analytical Methods. Infrared absorption spectra were obtained with an AVATAR-320 FT-IR spectrometer (Nicolet). β-CD and CD ICs mixed with potassium bromide and pressed into pellets were devoted to IR measurements to examine the inclusion states of PFAs into β-CD. The spectra were recorded with an accumulation of 32 scans with a resolution of 4 cm^{-1}.

Wide-angle X-ray diffraction (WAXD) patterns of the samples were recorded on the imaging plate equipped on a RINT-2000 diffractometer (Rigaku Co.) with Ni-filtered Cu Kα radiation. The applied voltage and current were set to 40 kV and 50 mA, respectively. The exposure time for CD ICs was set 30 min, while that for β-CD was 10 min.

Thermogravimetric analysis (TGA) of guest molecules, β-CD, and CD ICs were acquired with a Shimadzu TGA-50 in the temperature range up to 900 °C at a heating rate of 10 °C/min. Differential scanning calorimetry (DSC) was performed with a Shimadzu DSC-60 in the temperature range between −50 and 250 °C at a heating rate of 10 °C/min. For both thermal analyses, dried nitrogen was used as the purge gas.

Results and Discussion

Characterization of Inclusion Compounds. When guest molecules contain hydrogen atoms, stoichiometries of CD ICs can be readily determined by solution ^{1}H NMR.[6,7] However, PFAs do not contain hydrogen atoms, and they are insoluble in

common organic solvents. Hence, the stoichiometries for C_9F_{20}/β-CD and $C_{20}F_{42}$/β-CD were determined by elemental analysis. The absolute values of weight for carbon, hydrogen, and fluorine include uncertainties due to the hygroscopicity of CD ICs. In contrast, the carbon/fluorine (C/F) ratios are reliable because the ratios determined from the mass percents for carbon and fluorine are not influenced by the hydrogen and oxygen masses from water molecules. The experimental C/F value for C_9F_{20}/β-CD is 2.99 (C, 36.70%; F, 12.24%) while the calculated values for the 1:1, 1:2, and 1:3 complexes of C_9F_{20} and β-CD are 1.61, 2.94, and 4.27, respectively. The molar ratio of C_9F_{20} to β-CD in the IC can thus be determined to be 1:2. This ratio is reasonable from the viewpoint of molecular sizes. The depth of a β-CD cavity is known as 7.9 Å[2,3] while the size of C_9F_{20} in the long-axis direction (15.2 Å) is twice as large as β-CD. These geometries were obtained using the density functional theory (DFT) with the B3LYP functional and the 6-31G* basis set.[41] Although unfluorinated *n*-alkanes generally take all-trans conformation, *n*-PFAs are likely to form a loose helical conformations in which the torsion angles composed of four adjacent carbons are ca. 164°. This is due to the steric hindrance or electrostatic repulsion among neighboring fluorines.[45] On the other hand, the experimental C/F value for $C_{20}F_{42}$/β-CD is 2.91 (C, 39.03%; F, 13.39%), whereas the calculated C/F values for 1:3, 1:4, and 1:5 complexes of $C_{20}F_{42}$ and β-CD are 2.20, 2.83, and 3.46, respectively. The ratio for 1:4 complex shows good agreement, and it is reasonable in the light of the molecular sizes: the length of $C_{20}F_{42}$ along the long-axis is estimated as 29.2 Å, which is larger by a factor of 4 compared with the depth of a β-CD cavity. A slightly larger experimental value of C/F suggests that β-CDs including no $C_{20}F_{42}$ are misaligned in $C_{20}F_{42}$/β-CD. In contrast, the experimental results suggest that β-CD does not form a complex with the solvent used.

FT-IR spectroscopy is useful in determining the inclusion states of CD ICs, in particular for case where a guest molecule has a carbonyl group[10,18] because the carbonyl-stretching band is sensitive to conformational changes of the guest and hydrogen-bond formation between the guest and host CD. Figure 1 shows the FT-IR spectra of β-CD, C_9F_{20}, $C_{20}F_{42}$, and their ICs in the region from 400 cm^{-1} to 1550 cm^{-1}. The most striking features for PFAs are the three intense bands appearing at 1240, 1210, and 1153 cm^{-1} (bands 1 to 3).[46−50] For structural analysis, we focused on these bands because all other bands of PFAs are overlapped with the strong absorption of β-CD. First, both bands 1 and 3 are ascribed to the E_1 fundamental mode of PTFE, whose transition dipole moment is perpendicular to the molecular long axis. According to the reported assignments,[47−49] band 1 is attributed to the antisymmetric CF_2 stretching and the CF_2 rocking vibration, while band 3 to the symmetric CF_2 stretching and the CF_2 scissoring vibration. On the other hand, band 2 is ascribed to A_2 fundamental mode, whose transition dipole moment is parallel to the molecular long axis and arising from the C−C−C bending and C−C stretching motions.

By the way, quantum chemical calculations have predicted that PFAs (*n*-C_4F_{10} to C_6F_{14}) can take multiple conformers called *gauche* (the torsion angle consisting of four neighboring carbons is ca.54°), *ortho* (95°), and *anti* (165°).[51,52] Although other conformers specified by different sets of torsion angles have also been proposed for *n*-$C_{20}F_{42}$,[45] *anti* is actually the most stable conformer. In fact, it has been reported that there can be considerable *gauche* and little *ortho* in gaseous *n*-C_4F_{10} based on the IR measurement of isolated *n*-C_4F_{10} in nitrogen matrix deposited on the cryogenic window.[53] In that case, three intense bands were also observed at 1253, 1230, and 1149 cm^{-1}, in

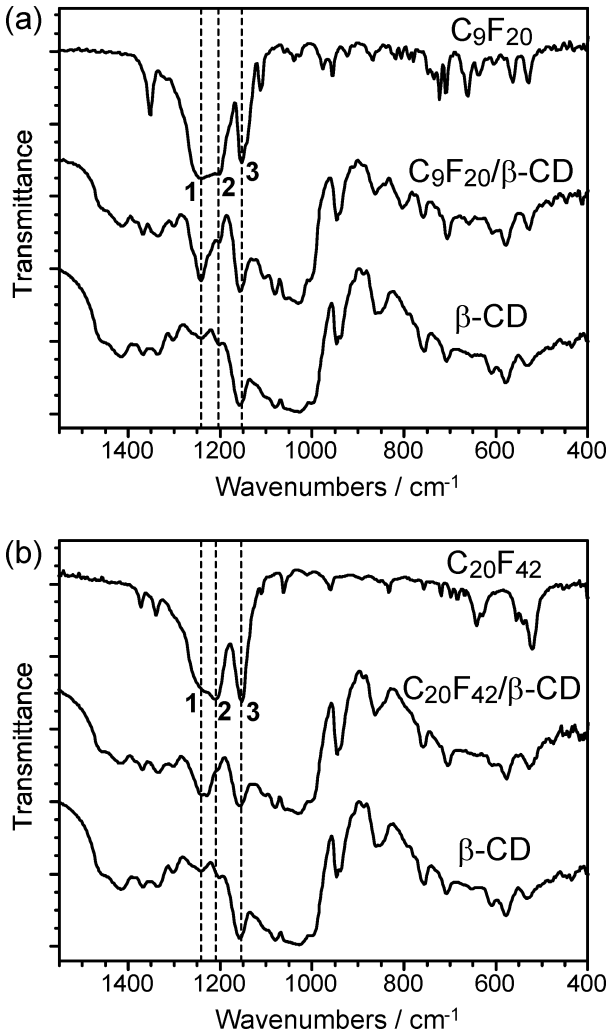

Figure 1. Comparison of FT-IR spectra: (a) C_9F_{20}, C_9F_{20}/β-CD, and β-CD; (b) $C_{20}F_{42}$, $C_{20}F_{42}$/β-CD, and β-CD.

which the 1230 cm^{-1} band was attributed only to the *anti* conformer. Attention will now be given to the spectrum of C_9F_{20}/β-CD. This is not simply the superposition of the spectra of neat C_9F_{20} and pure β-CD. While band 1 is clearly observed, band 2 has almost disappeared. Incidentally, band 3 of C_9F_{20}/β-CD is indistinguishable from another strong band of β-CD at 1157 cm^{-1}. The same features are observed for the IR spectrum of $C_{20}F_{42}$/β-CD compared with that of $C_{20}F_{42}$. Although the C_9F_{20} and $C_{20}F_{42}$ molecules included in β-CD are different from the C_4F_{10} trapped on a cold window not only in the molecular size but also in the reported vibrational assignments,[47−49,53] they are similar in the sense that PFA molecules are isolated from each other. Accordingly, we infer that the significant decrease in the intensities of band 2 for PFA/β-CDs is related to the conformational changes of PFA molecules from *anti* to *gauche*. In fact, the inner diameter of β-CD cavity is close to the size of naphthalene molecule along the longer axis. Comparing the geometries of a *gauche* PFA with that of a naphthalene on graphical software (Chem3D, CambridgeSoft), the cross-sectional diameter of the *gauche* PFA is smaller than the long-axis of naphthalene. Hence, the *gauche* PFA can be fit to the inside space of β-CD channels. This hypothesis will be reconsidered below with the aid of solid-state ^{19}F MAS NMR and ^{19}F magnetic shielding calculations. At this moment, the observed changes indicate at least that the formation of β-CD ICs can be monitored from the IR signals for PFA guests.

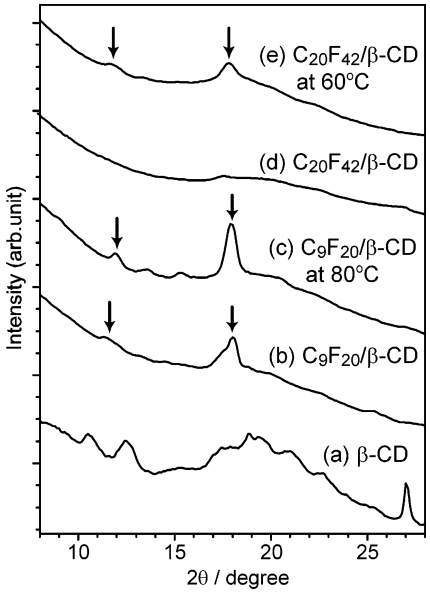

Figure 2. WAXD patterns of β-CD (a), C_9F_{20}/β-CD (b and c), and $C_{20}F_{42}/\beta$-CD (d and e). a, b, and d were obtained at ambient temperature.

Figure 2 shows the WAXD patterns for β-CD crystal, C_9F_{20}/β-CD, and $C_{20}F_{42}/\beta$-CD. The diffraction pattern for β-CD crystal (a) exhibits two major peaks at $2\theta = 12.4$ and 10.5° with many minor peaks from cage-type arrangement of β-CD molecules.[3,21] For C_9F_{20}/β-CD (b), two major peaks are observed at $2\theta = 17.8$, 11.6°, corresponding to the spacings of the crystalline lattices with 5.0, 7.6 Å, respectively. Note that 5.0 Å is close to the distance between the adjacent cylindrical alignments of β-CD molecules, which suggests that C_9F_{20}/β-CD forms the 'channel-type' crystal.[3,21] An additional remark is that the another lattice with 7.6 Å is consistent with the height of single β-CD molecule (7.9 Å). In contrast, no characteristic reflections are observed for $C_{20}F_{42}/\beta$-CD in this angular region (d), indicating that $C_{20}F_{42}/\beta$-CD does not have long-range ordered structures, and more specifically, it is nearly amorphous. The morphological difference between C_9F_{20}/β-CD and $C_{20}F_{42}/\beta$-CD is also reflected in the appearance of samples: the former is powdery, but the latter is flaky. The variation in the diffractograms by temperature (from b to c and d to e in Figure 2) will be described below.

The thermogravimetric analysis (TGA) curves for β-CD, C_9F_{20}/β-CD, and $C_{20}F_{42}/\beta$-CD are shown in Figure 3, in which the curves are normalized by the residual weight of each sample at 100 °C to neglect the weight loss arising from moisture desorption. Interestingly, both ICs gradually lose their weight by a few percent while pure β-CD keeps its weight at 100 °C up to ca.300 °C at which significant degradation begins. The weight loss is most likely due to the evaporation of crystal water loosely bound to ICs because it is difficult to account for by a volatilization of incorporated PFAs. If C_9F_{20} molecules escape from β-CD cavities as vapor at temperatures below 300 °C, the weight loss of the IC should be the mass fraction of C_9F_{20} in the ICs. In case that C_9F_{20}/β-CD contains no crystal water, the calculated mass fraction of C_9F_{20} in the IC approaches ca. 20%. However, the ICs hardly lose their weights even if they are kept at 250 °C, which is well above the boiling point of pure C_9F_{20} (125 °C) (TGA curve is not shown). This indicates that PFAs once included in β-CD cavities scarcely evaporate until temperatures at which β-CD pyrolytically decomposes (ca. 300 °C). The 5% weight loss temperatures for β-CD and C_9F_{20}/β-CD are 296 °C and 291 °C, respectively, whereas that for $C_{20}F_{42}/\beta$-CD is 276 °C. The lower decomposition temperature for

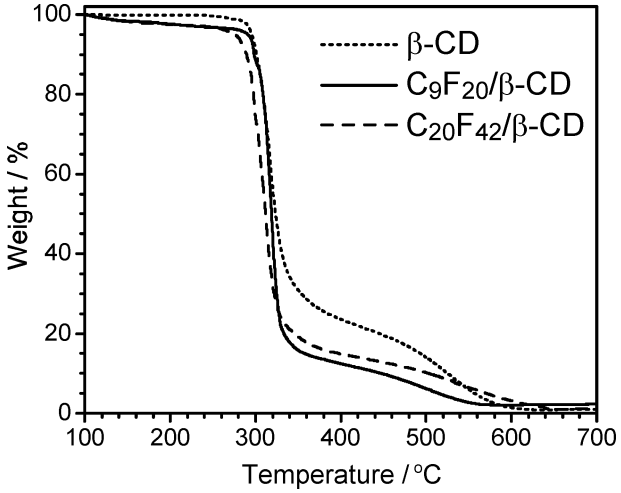

Figure 3. TGA curves for β-CD, C_9F_{20}/β-CD, and $C_{20}F_{42}/\beta$-CD. The weight loss is normalized by the weight of each sample at 100 °C.

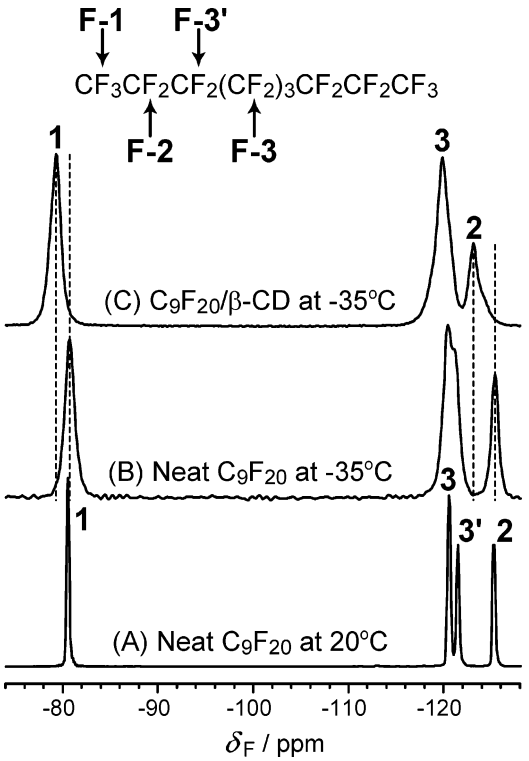

Figure 4. (A) Liquid-state ^{19}F NMR spectrum of C_9F_{20} under the static condition. Experimental parameters: data points, 4096; recycle delay, 30 s; 16 transients. (B) ^{19}F direct polarization (DP) MAS NMR spectrum of freezed C_9F_{20}. Experimental parameters: MAS rate, 15 kHz; data points, 2048; recycle delay, 30 s; 128 transients. (C) ^{19}F DP MAS NMR spectrum of C_9F_{20}/β-CD at the same condition as (B) except for 5 s of recycle delay and 64 transients.

$C_{20}F_{42}/\beta$-CD may be caused by the lower crystallinity, which also reflects the fact that β-CD and C_9F_{20}/β-CD are highly crystalline but $C_{20}F_{42}/\beta$-CD is nearly amorphous.

Neat C_9F_{20} and C_9F_{20}/β-CD. ^{19}F direct polarization (DP) MAS NMR spectra for neat C_9F_{20} and C_9F_{20}/β-CD are shown in Figure 4 with the signal assignments. The ^{19}F spectrum of liquid-state C_9F_{20} (A) was obtained at 20 °C under static condition. According to the literature,[51] the signals are assigned as follows: −80 ppm (peak 1), CF_3 group (F-1); −125 ppm (peak 2), CF_2 group next to the terminal CF_3 (F-2); −121 ppm (peak 3), central CF_2 group (F-3). In addition, another signal is observed on the right-hand side of peak 3 (denoted as peak 3′).

As might be expected, the ratio of the integrated intensities agrees well with the ratio of the number of fluorines (peak 1:peak 3:peak 3′:peak 2 = 3:3:2:2). Figure 4B shows the ^{19}F DP MAS NMR spectrum of C_9F_{20} measured at −35 °C at a spin rate of 15 kHz. Cooling below the freezing temperature (−16 °C) of C_9F_{20} gives rise to signal broadening and spinning sidebands (not shown in Figure 4) originating from insufficient motional averaging of ^{19}F homonuclear dipolar couplings and ^{19}F chemical shift anisotropy. As a result, the ratio of the integrated intensities for the isotropic peaks (peak 1:peak 3:peak 3′: peak 2 = 3.7:3.2:2:2) do not agree with the ratio of 3:3:2:2. Note that the chemical shift of each signal at −35 °C accords well with that at 20 °C. On the other hand, all the signals for C_9F_{20}/β-CD resonate at higher frequencies by 1.4−2.3 ppm than those for neat C_9F_{20} at the same temperature as shown in Figure 4C. Since peak 3′ merges with peak 3 at the lower temperature, both peaks will be treated together as peak 3 in the following discussion. The variation in chemical shift of each signal for C_9F_{20}/β-CD with respect to that of neat C_9F_{20} is as follows: peak 1, +1.4 ppm; peak 2, +2.3 ppm; peak 3, +0.6 ppm. One can also notice that the line width of each signal in C is fairly broad compared to that in B. Moreover, the line shape of peak 2 in C is somewhat distorted, while that in (B) can be fitted by single Lorentzian curve. These spectral features suggest that C_9F_{20} is not homogeneously arranged in the β-CD channel, or some guest molecules may not be completely covered with β-CD.

An important finding here is that the inclusion by β-CD has a strong influence on the ^{19}F chemical shifts of C_9F_{20}. What are the causes for the higher-frequency shifts of ^{19}F signals? In general, the ^{19}F chemical shifts sensitively reflect conformational differences in the solid state. Actually, it is well-known that poly(vinylidene fluoride) (PVDF) can take both *gauche* and *trans* conformations and that the fluorines located at the *gauche* position resonate at higher frequency by ca.15 ppm than those at the *trans*.[35] As a matter of fact, PFAs can also take a couple of conformations as mentioned above.[45,51−53] However, to our knowledge, no indication has ever been reported on the distinction of the conformers for PFAs by ^{19}F MAS NMR. This is because the perfluoroalkyl chains in PFAs are highly mobile with respect to timescales of NMR; a series of papers has reported that *n*-$C_{20}F_{42}$ can undergo not only rotational motion about their long axes but translational motion even at 200 K.[54−56] In fact, the ^{19}F chemical shift shown in Figure 4B originates from the time-averaged conformers having the Boltzmann distribution. Hence, under the assumption that each conformer intrinsically possessed different ^{19}F shieldings, an increase in the fraction of *gauche* conformers could cause chemical shift changes. To estimate the differences in ^{19}F shieldings between these conformers, the magnetic shielding calculations using DFT were performed with the B3LYP functional and the 6-311+G-(2d, p) basis set for *anti* and *gauche* conformers.[41] We did not take the *ortho* conformer into account because it is much less stable than the others.[51−53] Prior to the shielding calculations, the geometric structures of the conformers were fully optimized with 6-31G(d) basis set, as summarized in Table 1. The schematic illustrations are shown in Scheme 1. It should be noted that a "*gauche*" conformer consists of alternate dihedral angles (ca.55° and ca.164°). Hence, to be precise, the conformer should be called "*anti-gauche*", but we call it "*gauche*" here for simplicity. The estimated length along the long-axis for the *gauche* conformer is 14.1 Å, which is shorter than that for *anti* by 1.1 Å. The relative energy difference between the *gauche* and the *anti* is 4.1 kJ/mol. The calculated shieldings and the differences are listed in Table 2. To be sure, the absolute shieldings for *gauche* conformer are larger than those for *anti* except F-2, but the differences are too small to separate *gauche* from *anti* by chemical shift. In other words, it is difficult to ascribe the observed shift of 1.4−2.3 ppm only to the conformational changes.

TABLE 1: Optimized Dihedral Angles (deg) for Two Conformers of *n*-C_9F_{20} by DFT Calculations (B3LYP/6-31G*)

	conformer	
constituent[a]	*gauche*	*anti*
$C^1-C^2-C^3-C^4$	55.0	164.6
$C^2-C^3-C^4-C^5$	164.1	163.2
$C^3-C^4-C^5-C^6$	54.5	162.9
$C^4-C^5-C^6-C^7$	164.3	162.9
$C^5-C^6-C^7-C^8$	54.6	163.2
$C^6-C^7-C^8-C^9$	166.0	164.6

[a] The carbon atoms are numbered as superscripts, starting from one end and going to the other.

SCHEME 1: The Schematic Illustrations of *Gauche* and *Anti* Conformers

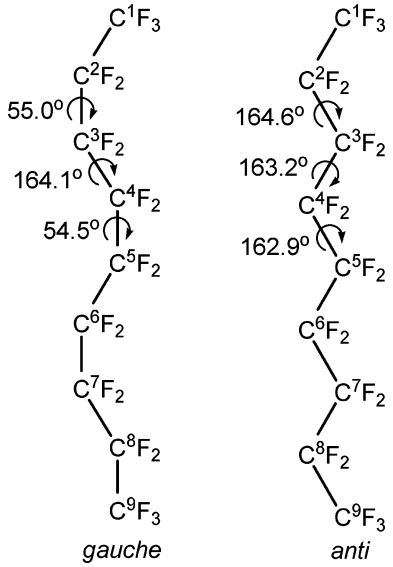

Another presumable factor that causes chemical shift change is 'dielectric media effect' or so-called solvent effect frequently observed in solution-state NMR: peak positions of a solute are affected by the dielectric effect of a solvent. Since the inside of a CD cavity is less polar and more hydrophobic than the outside,[2] molecules incorporated in CDs should exist in such an environment. In fact, the same effect has been validated for the ICs consisting of α-CD and benzene derivatives by ^{13}C NMR and semiempirical molecular orbital calculations.[31] In this study, the observed chemical shift differences were not quantitatively reproduced but qualitatively explained by considering two media having different dielectric constants. Dielectric media effect may predominantly contribute to the higher-frequency shift of ^{19}F signals, although conformational change from *anti* to *gauche* cannot be denied as suggested by FT-IR.

The variable temperature (VT) ^{19}F DP spectra for C_9F_{20}/β-CD are shown in Figure 5. Overall and monotonous peak shifts to the higher-frequency side are observed with increasing temperature, which simply comes from the nature of the probe. This may originate from the temperature dependence of electronic circuits. This shift is estimated to be less than 0.02 ppm/K in the temperature range between −40 and 80 °C and does not reflect any changes in molecular structure or dynamics

TABLE 2: ^{19}F Magnetic Shieldings Calculated by B3LYP/6-311+G(2d, p)

	^{19}F magnetic shielding (ppm)			
conformer	F-1	F-2	F-3′	F-3
gauche	254.16	300.37	297.24	296.24
anti	253.89	300.62	295.98	295.59
difference[a]	+0.27	−0.25	+1.26	+0.65

[a] Difference in shieldings for *gauche* conformer with respect to those for *anti* conformer.

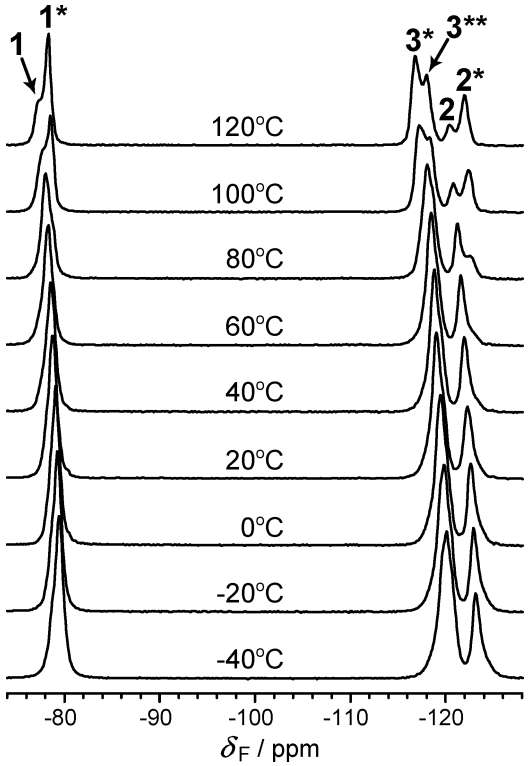

Figure 5. ^{19}F DP MAS NMR spectra of C_9F_{20}/β-CD at various temperatures. A ^{19}F spin-lock for 1 ms was applied to before data acquisition to eliminate the distorted baseline.

of samples. An important finding here is that new signals, which are distinguishable from peaks 1 to 3, appear above 80 °C and gradually increase their intensities with increasing temperature. The new peaks are denoted with asterisks in the figure. At 120 °C, peaks 1* and 2* resonate at lower frequencies by 1.0 and 1.6 ppm than peaks 1 and 2, respectively. In fact, the tail observed at the right-hand side of peak 2 appears to increase its intensity, leading to peak 2*. In contrast, peaks 3* and 3** seem to grow up at the both sides of peak 3 when we neglect the gradual high-frequency shifts. Considering that peak 3 still exists between peaks 3* and 3**, the peaks observed at 120 °C can be fitted well by Gaussian functions (see Supporting Information). This is in contrast to the neat C_9F_{20} in the frozen state (below the melting temperature, Figure 4B) for which the ^{19}F signals are well fitted by Lorentzian functions even though their line widths are nearly the same as those for C_9F_{20}/β-CD. By use of the integrals of decomposed peaks, the proportions of the newly appearing signals to the total intensity were calculated. Peak 1* including its spinning sidebands amounts to 59% of the total F-1 signals. In the same way, peak 2* reaches 64% of the total F-2 signals, while peaks 3* and 3** amount to 64% of the total F-3 signals. That is, approximately 60% of C_9F_{20} molecules turn out to be in another environment up to 120 °C, resulting in two unexchangeable sites on the spectral time scale. In other words, the fluorines corresponding to peaks

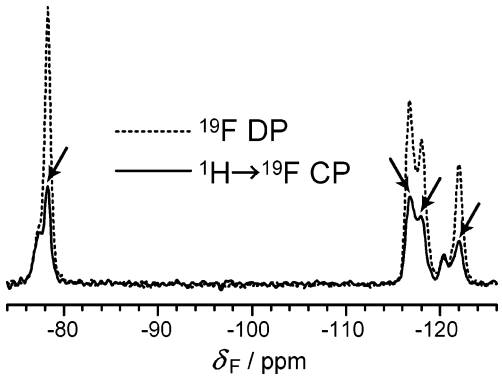

Figure 6. ^{1}H→ ^{19}F CP/MAS spectrum of C_9F_{20}/β-CD at 120 °C with a contact time of 0.1 ms (solid line). Arrows point the signals appearing above 80 °C. Dotted line shows ^{19}F DP MAS spectrum for comparison. The signal intensities in both spectra are normalized by peak 2.

1* to 3** are distinctly different in molecular motion and structure from those to peaks 1 to 3.

The spectral changes caused by heating are almost reversible, although they require time to retrieve the former state (see Supporting Information). For instance, when the sample temperature jumped from 40 to 120 °C, it requires approximately 2 h to provide the same spectral shape as shown in Figure 5. In contrast, when the sample was quenched from 120 °C to 40 °C, it takes at least 2 days to be restored. Since TGA and DSC measurements suggest that a significant amount of crystal water is incorporated in PFA/β-CD ICs, time-consuming changes observed for the ^{19}F line shape are due to structural transformations in C_9F_{20}/β-CD, which involve the processes of desorption and adsorption of crystal water. In fact, the reversible crystal transitions induced by hydration and/or dehydration have been reported for other CD ICs.[57−58] As dehydration proceeds as the temperature increases, CD molecules can readily rearrange accompanied by guest molecules rather than keeping a specific crystal system. In cases of reported crystal transitions, CD channels simply rearranged in the perpendicular direction to the channel axis, while on the other hand, it is reasonable to consider that C_9F_{20}/β-CD rearranges in the direction along the channel axis. Here, we focus our attention on the WAXD pattern for C_9F_{20}/β-CD observed at 80 °C as shown in Figure 2c. Compared with the pattern at ambient temperature (b), the diffraction peaks become distinct, suggesting that the crystal lattices become more ordered. In addition, the peak at $2\theta = 11.6°$ is displaced to the wide-angle side by 0.3°, indicating the shrinkage of the lattice spacing associated with β-CD stacking by approximately 0.2 Å. Further increases in the temperature until 120 °C simply provide more intense peaks at the same angles.

Now let us return to Figure 5. Neglecting the gradual high-frequency shifts by raising the temperature, the chemical shifts of peaks 1* to 3** for C_9F_{20}/β-CD at 120 °C are close to those of peaks 1 to 3′ for neat C_9F_{20}. More specifically, peaks 1* and 2* appear at the lower-frequency side than peaks 1 and 2, respectively. Besides, peaks 3* and 3** are distinguishable just like peaks 3 and 3′ for neat C_9F_{20}. However, peaks 1* to 3** cannot be ascribed to the fluorines of isolated C_9F_{20} because C_9F_{20} molecules scarcely escape from the β-CD channel as indicated by the TGA measurements. Additionally, if C_9F_{20} is vaporized, the above-mentioned changes in ^{19}F line shapes by temperature would not be reversible.

A ^{1}H→^{19}F CP/MAS experiment was performed to examine the nature of the newly appearing signals. Figure 6 shows the ^{1}H→^{19}F CP/MAS NMR spectrum of C_9F_{20}/β-CD (solid line)

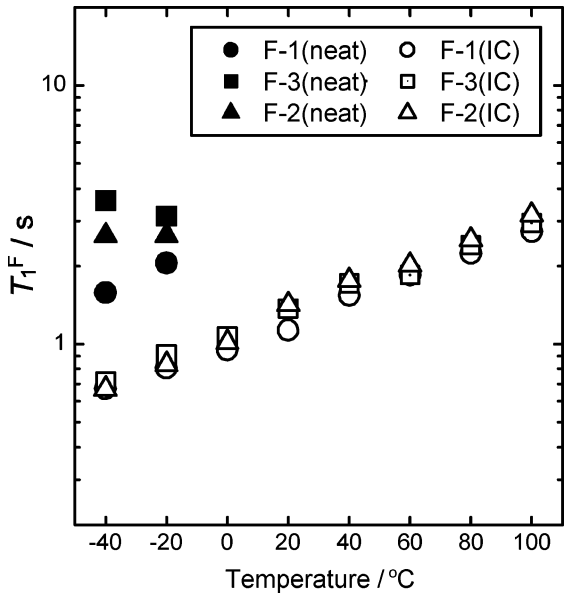

Figure 7. Temperature dependence of T_1^F value for each signal in Figure 4: filled symbols, neat C_9F_{20}; open symbols, C_9F_{20}/β-CD.

obtained at 120 °C with a contact time of 0.1 ms, in which the signals of the fluorines located at relatively immobile sites or in components close to the protons are preferentially observed. Comparing with the ^{19}F DP spectrum (dotted line) normalized by the intensity of peak 2, peaks 1* to 3** (pointed by arrows in the figure) are weakened in the CP spectrum, while peak 1 keeps its intensity. By comparison, the line shape of the $^1H \rightarrow ^{19}F$ CP/MAS NMR spectrum was almost the same as that of ^{19}F DP spectrum at room temperature. Accordingly, peaks 1* to 3** are assignable to the fluorines located in components distant from protons of β-CD. This is reasonable because the uncovered parts of C_9F_{20} must be relatively more distant from β-CD than the C_9F_{20} included in β-CD. In addition, the uncovered parts are supposed to be much more mobile than the covered parts.[10] To be brief, it is likely that β-CD channels are reconstructed by vaporization of crystal water, while C_9F_{20} partly comes out of the edges of β-CD channels. This explanation seems reasonable from the viewpoint that the attractive interactions between C−F bonds in PFA and C−H bonds in β-CD cavity should be weak.

Figure 7 gives the variation of ^{19}F spin-lattice relaxation times in the laboratory frame (T_1^F) as a function of temperature, in which T_1^F values for C_9F_{20}/β-CD and C_9F_{20} are plotted by open and solid symbols, respectively. For clarity and simplicity, the T_1^F of the fluorines appearing only at higher temperature (peaks 1* to 3**) are not shown. As is evident from Figure 7, the T_1^F values for F-1 to F-3 for C_9F_{20}/β-CD are close to each other at each temperature, while those for C_9F_{20} are different. Note that the T_1^F values of C_9F_{20}/β-CD are smaller than those of neat C_9F_{20}, which suggests that the relaxation of F-1 at CF_3 group occurs more effectively in C_9F_{20}/β-CD than in neat C_9F_{20}.

Spin-lattice relaxation of spin-1/2 like ^{19}F is caused by the fluctuation of the local field, which consists of the large static field and the small local interactions (usually dipolar couplings or chemical shift anisotropies) fluctuating with molecular motions at the site. The most efficient relaxation occurs at a certain correlation time of the fluctuation where the spectral density of the Larmor frequency is the highest. To be brief, the T_1 value comes to a minimum when the molecular motions on the Larmor time scale (several hundreds of MHz) are sufficiently present in the system.[59] In case of PFAs, one of the motions on the Larmor time scale is the internal rotation of the terminal CF_3 (F-1) around a threefold axis, which will result in the lowest T_1^F value of the three in the absence of dipolar coupling with other fluorines. It is indeed true of neat C_9F_{20}. In contrast, the T_1^F values of fluorine spins coupled via dipolar interaction will match the smallest of them by efficient spin diffusion, irrespective of the intrinsic molecular motions. It is the case of C_9F_{20}/β-CD.

What makes the spin diffusion in neat C_9F_{20} insufficient? In general, motions that are faster than the Larmor time scale such as libration of C−F bonds and vibrations of other bonds can eliminate intramolecular dipolar couplings between fluorines.[59] In such a case ^{19}F spin diffusion hardly occurs, resulting in the specific relaxation times of fluorines at different moieties. It has also been reported that neat PFAs (C_6F_{14} to C_8F_{18}) demonstrate the same T_1^C values for the CF_2 carbons and the smaller T_1^C value for the CF_3 carbon by ^{13}C solution NMR.[60] Since ^{13}C is a rare spin, and hence the spin diffusion hardly occurs, the proximity of carbon atoms does not affect the T_1^C values unlike abundant spins such as ^{19}F and ^1H. Accordingly, the agreement in the T_1^C for the CF_2 straightforwardly implies the motional restriction of carbon skeleton even in liquid while the lower T_1^C for the CF_3 is indicative of the rotational motion around threefold axis. This means that the vibrational motion of C−C bond is not expected and that only the librational motion of C−F bond can be responsible for averaging dipolar coupling between the fluorines.

Attention should be given to the plots for C_9F_{20}/β-CD in the figure, where the T_1^F values of F-1 to F-3 coincide well at each temperature. This is due to effective spin diffusion as mentioned above. The values of around 1 s at lower temperatures seem close to the T_1^F minimum, although we could not find a bottom for the limitation of the apparatus. This is because of the efficient relaxation via the internal rotation of CF_3 group on the Larmor time scale, which also indicates that the rotational motion is not hindered by the β-CD cavity. On the contrary, the motion in the β-CD channel is closer to the Larmor time scale than in the neat C_9F_{20} because of the lower T_1^F values. Needless to say, the good agreement in values also means that the homonuclear dipolar coupling between F-1 and F-2 is present despite the rotational motion of the CF_3 group. As a matter of fact, it is not surprising because only faster motions than the Larmor time scale can average certain terms of dipolar interactions that are related to magnetic relaxation.[59] In other words, the rotational motions that are typically on the Larmor time scale or slower do not influence the spin diffusion. A monotonic increase in the T_1^F values with increasing temperatures is indicative of a decrease in the fraction of rotational motion on the Larmor time scale; the motion is getting faster. However, it is quite unlikely to behave like liquid or in the rotator phase at least in the temperature range for the measurements because both ^{19}F spin diffusion and $^1H \rightarrow ^{19}F$ CP still effectively occur. At 100 °C, the T_1^F values for all the peaks range from 2.1 to 3.1 s. Unfortunately, the difference in the T_1^F values for peaks 1 and 1* (2.1 s), or that for peaks 3, 3*, and 3** (2.7 s) is indistinguishable due to the spectral spin diffusion. However, that for peak 2 (3.1 s) is significantly different from that for peaks 2* (2.1 s), indicating that the fluorines assignable to peaks 2 and 2* are located at different parts in molecular motion.

If the C_9F_{20} molecules included in β-CD channels undergo slower motions such as conformational exchanges or overall rotation along the molecular axis, such motions would be detected by the ^{19}F spin-lattice relaxation times in the rotating frame ($T_{1\rho}^F$). The values take a minimum in the presence of sufficient molecular motions on the spin-lock frequency (100

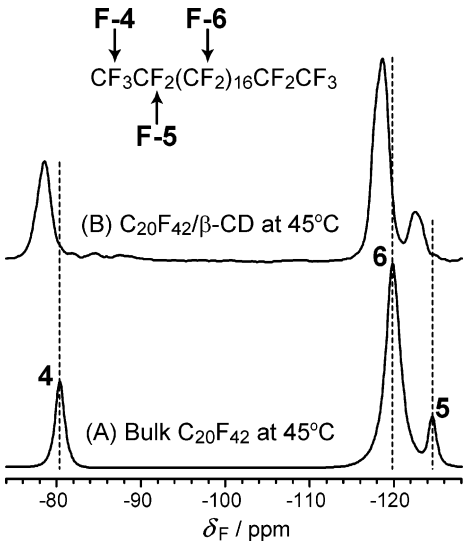

Figure 8. (A) ^{19}F DP MAS NMR spectrum of $C_{20}F_{42}$. Experimental parameters: recycle delay, 30 s; 16 transients. (B) ^{19}F DP MAS NMR spectrum of $C_{20}F_{42}/\beta$-CD. Experimental parameters: recycle delay, 6 s; 128 transients.

kHz in this study). As expected, the $T_{1\rho}{}^{F}$ values for neat C_9F_{20} are too large to estimate exact values. However, even for C_9F_{20}/β-CD, the values are estimated as longer than 20 ms (the longest spin-lock time applied) at every temperature. This indicates that the molecular motions at around 100 kHz are not vigorous, and C_9F_{20} does not undergo overall rotation in the β-CD channels.

Neat $C_{20}F_{42}$ and $C_{20}F_{42}/\beta$-CD. The ^{19}F DP MAS NMR spectra for neat $C_{20}F_{42}$ and $C_{20}F_{42}/\beta$-CD are shown in Figure 8 with the signal assignments. By analogy with long-chain fluoroalkyl surfactants,[28] the fluorine signals for neat $C_{20}F_{42}$ are assigned as follows: −80 ppm (peak 4), CF_3 group (F-4); −124 ppm (peak 5), CF_2 group next to the terminal CF_3 (F-5); −120 ppm (peak 6), central CF_2 group (F-6). Because of the longer chain, peak 6 shows no fine structure like that of peaks 3 and 3′ of C_9F_{20}. Just like C_9F_{20}/β-CD, all the signals for $C_{20}F_{42}/\beta$-CD resonate at higher frequencies by 1.2−2.1 ppm than those for neat $C_{20}F_{42}$ at the same temperature. The variation in chemical shift of each signal for $C_{20}F_{42}/\beta$-CD in comparison with that of neat $C_{20}F_{42}$ is as follows: peak 4, +1.8 ppm; peak 5, +2.1 ppm; peak 6, +1.2 ppm. The spectrum for neat $C_{20}F_{42}$ at 45 °C (A) can be fitted by single Lorentzian curve whereas that of $C_{20}F_{42}/\beta$-CD at the same temperature (B) contains Gaussian components to a certain extent. The difference in line shape suggests that each $C_{20}F_{42}$ molecule in neat is uniformly arranged in the crystal phase while ICs statistically consisting of one $C_{20}F_{42}$ and four β-CDs have structural disorder and/or distribution, which agree with the results of WAXD.

Figure 9 shows the VT ^{19}F DP (solid lines) and ^{1}H→^{19}F CP/MAS (dotted lines) spectra for $C_{20}F_{42}/\beta$-CD, in which all the spectra are normalized with the intensity of peak 4 resonating at ca.−80 ppm. Peaks 4 to 6 are displaced linearly to the higher frequency side with an increase in temperature, which is negligible as mentioned in Figure 5. Unlike the case of C_9F_{20}/β-CD, the spectral shapes of ^{19}F DP spectra do not show significant changes in the measurement temperature range. This suggests that most parts of $C_{20}F_{42}$ in β-CD will be included even at higher temperatures. In fact, comparing with the ^{1}H→^{19}F CP spectra reveals that a tiny shoulder at the right-hand side of peak 4 grows up to a peak as the temperature increases. This is similar to the behavior of peak 1* for C_9F_{20}/β-CD, indicating that the tiny peak is assignable to the fluorines uncovered by

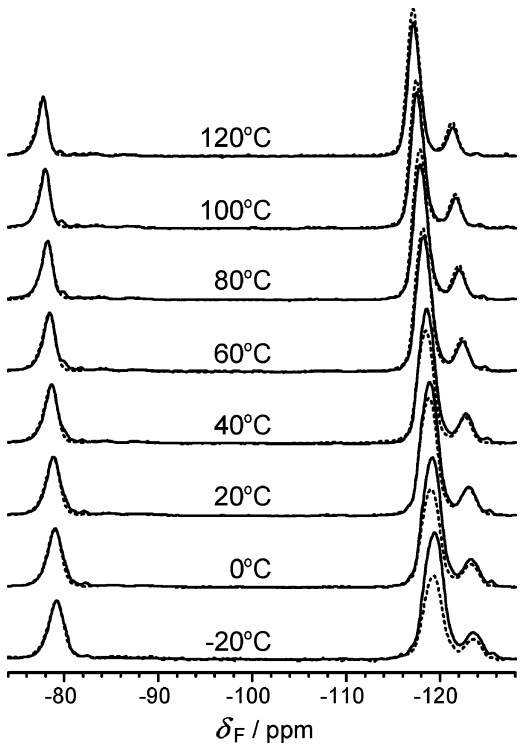

Figure 9. Variable-temperature ^{19}F DP MAS NMR spectra of $C_{20}F_{42}/\beta$-CD (solid lines). Experimental parameters: recycle delay, 10 s; 64 transients. Dotted lines show ^{1}H→ ^{19}F CP/MAS NMR spectra normalized by peak 4 at each temperature. Experimental parameters: contact time, 0.2 ms; recycle delay, 9 s; 128 transients.

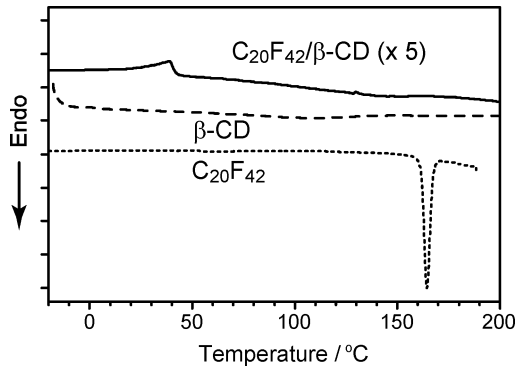

Figure 10. DSC curves for $C_{20}F_{42}/\beta$-CD, β-CD, and $C_{20}F_{42}$. The curve for $C_{20}F_{42}/\beta$-CD was magnified 5 times in a longitudinal direction for clarity.

β-CD. Another tiny signal near peak 5 will also act in a similar fashion if all the spectra are normalized with the intensity of peak 5.

On the other hand, the relative intensities of peak 6 based on those of peak 4 behave differently as increasing temperature: the relative intensities of the CP signals increase until 60 °C and then remain constant, while those of the DP signals are almost unchanged in the measurement temperature range. This means that the ^{1}H→^{19}F CP at a contact time of 0.2 ms becomes more efficient above 40 °C, which cannot be directly associated with the molecular dynamics exhibiting no contact-time dependence, but it should be related to some sort of structural changes as described below.

The DSC curves of $C_{20}F_{42}/\beta$-CD, pure β-CD, and neat $C_{20}F_{42}$ are summarized in Figure 10. Since the first heating curves exhibit a huge endothermic peak arising from the vaporization of crystal water, second heating scans are shown for $C_{20}F_{42}/\beta$-CD and β-CD. The curve for neat $C_{20}F_{42}$ demonstrates an

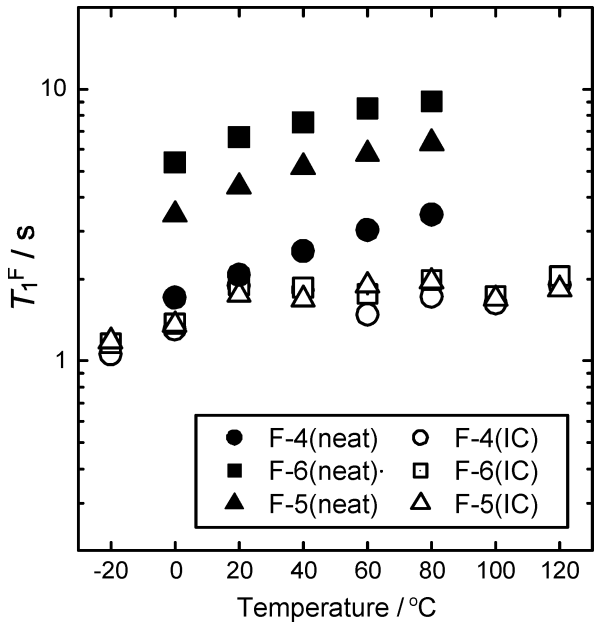

Figure 11. Temperature dependence of T_1^F value for each signal in Figure 8: filled symbols, neat $C_{20}F_{42}$; open symbols, $C_{20}F_{42}/\beta$-CD.

endothermic peak at 164 °C due to the fusion of the rhombohedral crystal.[54] In contrast, a similar endothermic peak is not shown in the curve for $C_{20}F_{42}/\beta$-CD because each $C_{20}F_{42}$ molecule is isolated by the β-CD cavities, and hence it does not form a crystal. However, $C_{20}F_{42}/\beta$-CD exhibits a weak exothermic peak at ca.40 °C, suggesting that a certain type of crystallization may occur at the temperature, and it leads to ordered structures.

To confirm the heating-driven structural changes, we now turn to the WAXD analyses. As has been shown in Figure 2d, the WAXD pattern of $C_{20}F_{42}/\beta$-CD exhibits no diffraction peaks, indicating that $C_{20}F_{42}/\beta$-CD is nearly amorphous. However, when $C_{20}F_{42}/\beta$-CD is kept at 60 °C, two peaks gradually appear in a few hours, which are pointed by arrows in Figure 2e. Note that the diffraction angles of the new peaks agree well with those of the most intense peaks for C_9F_{20}/β-CD, indicating that $C_{20}F_{42}/\beta$-CD also forms the channel-type crystal by annealing at 60 °C. When the sample is allowed to stand for more than 24 h, the WAXD pattern returned to the original feature. These time-consuming structural transformations should be accompanied by hydration and dehydration processes just like C_9F_{20}/β-CD.

Figure 11 shows the variations of T_1^F as a function of temperature, in which T_1^F values for $C_{20}F_{42}$ and $C_{20}F_{42}/\beta$-CD are plotted by solid and open symbols, respectively. As well as the cases for C_9F_{20} and C_9F_{20}/β-CD, the temperature dependence of T_1^F for $C_{20}F_{42}$ and $C_{20}F_{42}/\beta$-CD can be explained in terms of the internal rotation of CF_3 and the subsequent ^{19}F spin diffusion. For neat $C_{20}F_{42}$, the T_1^F values of F-4 to F-6 are completely different from each other at each temperature. This indicates that the homonuclear dipolar couplings and thereby the spin diffusion are ineffective, which originates from the librational motion of C−F bond. As expected, the magnetization of F-4 at CF_3 group relaxes more effectively than any other fluorine due to the rapid rotation around the local threefold axis. Moreover, the monotonic increase of each peak with an increase in temperature suggests that $C_{20}F_{42}$ molecules undergo molecular motions faster than the Larmor time scale in the measurement temperature range. This result is consistent with a reported knowledge that $C_{20}F_{42}$ in the rhombohedral phase is highly mobile and is free of orderliness about the helix handedness.[54−56]

In contrast, the T_1^F values for all fluorines of $C_{20}F_{42}/\beta$-CD are almost the same at each temperature. This indicates that the effective intramolecular spin diffusion occurs, which results from the suppression of librational motion at C−F bonds. The T_1^F values are in good agreement with those for F-4 in neat $C_{20}F_{42}$ at 0 °C and 20 °C, indicating that the principal relaxation path of ^{19}F magnetizations in $C_{20}F_{42}/\beta$-CD is the internal rotation at $-CF_3$ just like in neat $C_{20}F_{42}$. However, unlike the case of neat $C_{20}F_{42}$, in which the T_1^F values monotonically increase, the T_1^F values stay constant above 40 °C. It is noted that the transition point of the T_1^F values is consistent with the exothermic peak in the DSC curve. This is also close to the point at which the CP efficiency varies as demonstrated by VT $^1H\rightarrow^{19}F$ CP NMR spectra. Hence, the temperature dependence of T_1^F is closely related to the structural changes by annealing. The almost constant and small T_1^F values above 40 °C indicate that the rotational motion at $-CF_3$ group is still on the Larmor time scale even at the higher temperatures. This is an essential difference between C_9F_{20}/β-CD and $C_{20}F_{42}/\beta$-CD. The variations in $T_{1\rho}^F$ values as a function of temperature were obtained for both neat $C_{20}F_{42}$ and $C_{20}F_{42}/\beta$-CD, but the value in each case is much larger than the longest spin-lock time (20 ms). Accordingly, the molecular motions at ca.100 kHz are not vigorous even in $C_{20}F_{42}/\beta$-CD.

Conclusions

The inclusion compounds (ICs) consisting of β-cyclodextrin (β-CD) and two kinds of perfluoroalkanes (PFAs), C_9F_{20} and $C_{20}F_{42}$, were successfully prepared for the first time. The elemental analyses indicate that the molar ratio of C_9F_{20} to β-CD in C_9F_{20}/β-CD is 1:2, while that of $C_{20}F_{42}$ to β-CD in $C_{20}F_{42}/\beta$-CD is approximately 1:4. Both the ratios are reasonable from the view of molecular sizes estimated by quantum chemical calculations. For each IC, the specific IR absorption band associated with the vibrations along the longer axis of PFAs weakens, indicating that the formation of β-CD ICs can be monitored from the IR signals for PFA guests. The WAXD measurements revealed that C_9F_{20}/β-CD forms a channel-type crystal, while $C_{20}F_{42}/\beta$-CD is nearly amorphous at room temperature. Thermogravimetric analysis (TGA) demonstrated that the PFAs confined in the β-CD channel hardly evaporate or degrade unless the host is pyrolytically decomposed at 300 °C; inclusion by β-CD improves the thermal stability of PFAs remarkably. Differential scanning calorimetry (DSC) showed that a significant amount of crystal water is included in the ICs.

The ^{19}F NMR signals for PFA/β-CD ICs resonate at higher frequencies by approximately 1−2 ppm than those for neat PFAs. The variation in chemical shift can be predominantly caused by nonpolar environment of a β-CD cavity although the influence of conformational change of PFAs is not completely ignored. When C_9F_{20}/β-CD is heated above 80 °C, new ^{19}F signals appear at lower frequencies than the signals observed at low temperatures. Since these signals are not readily observed by $^1H\rightarrow^{19}F$ CP/MAS NMR, they are ascribed to the fluorines relatively distant from hydrogen atoms of β-CD or crystal water. As estimated from the peak areas, approximately 60% of C_9F_{20} is uncovered above 80 °C although the other part of C_9F_{20} still stays in the β-CD cavities. On the other hand, the DSC curve of $C_{20}F_{42}/\beta$-CD shows an exothermic peak at ca. 40 °C, suggesting that β-CD molecules rearrange at higher temperatures and form more ordered structures. Annealing of $C_{20}F_{42}/\beta$-CD at 60 °C for a few hours leads to a channel-type crystallite similar to C_9F_{20}/β-CD. These structural transformations are reversible but time-consuming because the hydration and/or

dehydration of crystal water are deeply involved in the formation and/or deformation of PFA/β-CD ICs. In summary, both PFA and β-CD molecules can rearrange in the direction of the channel at higher temperatures, which provides more ordered and tightly stacked ICs.

The ^{19}F spin-lattice relaxation times in the laboratory frame (T_1^Fs) for fluorines of neat PFAs are different, while those of PFA/β-CD ICs are close to each other. This is because the librational motion of C−F bond is effectively suppressed in the β-CD channel, and thereby ^{19}F spin diffusion readily occurs. The T_1^F values for PFA/β-CD ICs are smaller than those for the corresponding PFAs at every temperature, indicating that the internal rotation of the CF_3 group is on the Larmor time scale in the β-CD channel rather than hindered. The ^{19}F spin-lattice relaxation times in the rotating frame ($T_{1\rho}^F$s) for fluorines of PFA/β-CD ICs are too long to measure, suggesting that PFAs do not undergo the motions around 100 kHz like conformational changes and overall rotation about the molecular axis even in the β-CD channels.

Supporting Information Available: Experimental details. This material is available free of charge via the Internet at http://pubs.acs.org.

References and Notes

(1) Scheirs, J. In *Modern Fluoropolymers*; Scheirs, J., Ed.; John Wiley & Sons Ltd: Chichester, 1997.

(2) Szejtli, J. *Chem. Rev.* **1998**, *98*, 1743−1753.

(3) Harata, K. *Chem. Rev.* **1998**, *98*, 1803−1827.

(4) Nepogodiev, S. A.; Stoddart, J. F. *Chem. Rev.* **1998**, *98*, 1959−1976.

(5) Harada, A.; Li, J.; Nakamitsu, T.; Kamachi, M. *J. Org. Chem.* **1993**, *58*, 7524−7528.

(6) Harada, A.; Li, J.; Kamachi, M. *J. Am. Chem. Soc.* **1994**, *116*, 3192−3196.

(7) Fujita, H.; Ooya, T.; Yui, N. *Polym. J.* **1999**, *31*, 1099−1104.

(8) Girardeau, T. E.; Leisen, J.; Beckham, H. W. *Macromol. Chem. Phys.* **2005**, *206*, 998−1005.

(9) Lu, J.; Mirau, P. A.; Tonelli, A. E. *Macromolecules* **2001**, *34*, 3276−3284.

(10) Lu, J.; Mirau, P. A.; Daniel, Shin, I.; Nojima, S.; Tonelli, A. E. *Macromol. Chem. Phys.* **2002**, *203*, 71−79.

(11) Lu, J.; Mirau, P. A.; Tonelli, A. E. *Prog. Polym. Sci.* **2002**, *27*, 357−401.

(12) Rusa, C. C.; Wei, M.; Shuai, X.; Bullions, T. A.; Wang, X.; Rusa, M.; Uyar, T.; Tonelli, A. E. *J. Polym. Sci. B Polym. Phys.* **2004**, *42*, 4207−4224.

(13) Saalwächter, K. *Macromol. Rapid Commun.* **2002**, *23*, 286−291.

(14) Huang, L.; Allen, E.; Tonelli, A. E. *Polymer* **1998**, *39*, 4857−4865.

(15) Li, X.; Li, J.; Leong, K. W. *Polymer* **2004**, *45*, 6845−6851.

(16) Harada, A.; Li, J.; Suzuki, S.; Kamachi, M. *Macromolecules* **1993**, *26*, 5267−5268.

(17) Rusa, C. C.; Rusa, M.; Gomez, M.; Daniel, Shin, I.; Fox, J. D.; Tonelli, A. E. *Macromolecules* **2004**, *37*, 7992−7999.

(18) Dong, T.; He, Y.; Shin, K.; Inoue, Y. *Macromol. Biosci.* **2004**, *4*, 1084−1091.

(19) Rusa, C. C.; Uyar, T.; Rusa, M.; Hunt, M. A.; Wang, X.; Tonelli, A. E. *J. Polym. Sci. B Polym. Phys.* **2004**, *42*, 4182−4194.

(20) Uyar, T.; Rusa, C. C.; Hunt, M. A.; Aslan, E.; Hacaloglu, J.; Tonelli, A. E. *Polymer* **2005**, *46*, 4762−4775.

(21) Okumura, H.; Kawaguchi, Y.; Harada, A. *Macromolecules* **2001**, *34*, 6338−6343.

(22) Harada, A.; Li, J.; Kamachi, M. *Macromolecules* **1994**, *27*, 4538−4543.

(23) Avram, L.; Cohen, Y. *J. Org. Chem.* **2002**, *67*, 2639−2644.

(24) Sanji, T.; Kato, M.; Tanaka, M. *Macromolecules* **2005**, *38*, 4034−4037.

(25) Zhu, X.; Chen, L.; Yan, D.; Chen, Q.; Yao, Y.; Xiao, Y.; Hou, J.; Li, J. *Langmuir* **2004**, *20*, 484−490.

(26) Jiao, H.; Goh, S. H.; Valiyaveettil, S.; Zheng, J. *Macromolecules* **2003**, *36*, 4241−4243.

(27) Zhang, H.; Hogen-Esch, T. E.; Boschet, F.; Margaillan, A. *Langmuir* **1998**, *14*, 4972−4977.

(28) Guo, W.; Fung, B. M.; Christian, S. D. *Langmuir* **1992**, *8*, 446−451.

(29) Nostro, P. L.; Santoni, I.; Bonini, M.; Baglioni, P. *Langmuir* **2003**, *19*, 2313−2317.

(30) Druliner, J. D.; Wasserman, E. *J. Fluorine Chem.* **1995**, *72*, 75−78.

(31) Inoue, Y.; Hoshi, H.; Sakurai, M. Chujo, R. *J. Am. Chem. Soc.* **1985**, *107*, 2319−2323.

(32) Hall, L. D.; Lim, T. K. *J. Am. Chem. Soc.* **1986**, *108*, 2503−2510.

(33) Inoue, Y.; Okuda, T.; Chujo, R. *Carbohydr. Res.* **1983**, *116*, C5−C8.

(34) Garces, F. O.; Rao, V. P.; Garcia-Garibay, M. A.; Turro, N. J. *Supramol. Chem.* **1992**, *1*, 65−72.

(35) Holstein, P.; Scheler, U.; Harris, R. K. *Polymer* **1998**, *39*, 4937−4941.

(36) Ando, S.; Harris, R. K.; Reinsberg, S. A. *J. Magn. Reson.* **1999**, *141*, 91−103.

(37) Ando, S.; Harris, R. K.; Reinsberg, S. A. *Magn. Reson. Chem.* **2002**, *40*, 97−106.

(38) Aimi, K.; Ando, S. *Magn. Reson. Chem.* **2004**, *42*, 577−588.

(39) Aimi, K.; Ando, S.; Avalle, P.; Harris, R. K. *Polymer* **2004**, *45*, 2281−2290.

(40) Ando, S.; Harris, R. K.; Hazendonk, P.; Wormald, P. *Macromol. Rapid Comm.* **2005**, *26*, 345−356.

(41) Frisch, M. J.; Trucks, G. W.; Schlegel, H. B.; Scuseria, G. E.; Robb, M. A.; Cheeseman, J. R.; Montgomery, J. A., Jr.; Vreven, T.; Kudin, K. N.; Burant, J. C.; Millam, J. M.; Iyengar, S. S.; Tomasi, J.; Barone, V.; Mennucci, B.; Cossi, M.; Scalmani, G.; Rega, N.; Petersson, G. A.; Nakatsuji, H.; Hada, M.; Ehara, M.; Toyota, K.; Fukuda, R.; Hasegawa, J.; Ishida, M.; Nakajima, T.; Honda, Y.; Kitao, O.; Nakai, H.; Klene, M.; Li, X.; Knox, J. E.; Hratchian. H. P.; Cross, J. B.; Adamo, C.; Jaramillo, J.; Gomperts, R.; Stratmann, R. E.; Yazyev, O.; Austin, A. J.; Cammi, R.; Pomelli, C.; Ochterski, J. W.; Ayala, P. Y.; Morokuma, K.; Voth, G. A.; Salvador, P.; Dannenberg, J. J.; Zakrzewski, V. G.; Dapprich, S.; Daniels, A. D.; Strain, M. C.; Farkas, O.; Malick, D. K.; Rabuck, A. D.; Raghavachari, K.; Foresman, J. B.; Ortiz, J. V.; Cui, Q.; Baboul, A. G.; Clifford, S.; Cioslowski, J.; Stefanov, B. B.; Liu, G.; Liashenko, A.; Piskorz, P.; Komaromi, I.; Martin, R. L.; Fox, D. J.; Keith, T.; Al-Laham, M. A.; Peng, C. Y.; Nanayakkara, A.; Challacombe, M.; Gill, P. M. W.; Johnson, B.; Chen, W.; Wong, M. W.; Gonzalez, C.; Pople, J. *A. Gaussian 03*, revision C.02; Gaussian, Wallingford, CT, 2004.

(42) Brouwer, E. B.; Challoner, R.; Harris, R. K. *Solid State Nucl. Magn. Reson.* **2000**, *18*, 37−52.

(43) Aliev, A. E.; Harris, K. D. M. *Magn. Reson. Chem.* **1994**, *32*, 366−369.

(44) Bloch, F.; Siegert, *A. Phys. Rev.* **1940**, *57*, 522−527.

(45) Jang, S. S.; Blanco, M.; Goddard, W. A., III; Caldwell, G.; Ross, R. B. *Macromolecules* **2003**, *36*, 5331−5341.

(46) Liang, C. Y.; Krimm, S. *J. Chem. Phys.* **1956**, *25*, 563−571.

(47) Moynihan, R. E. *J. Am. Chem. Soc.* **1959**, *81*, 1045−1050.

(48) Rabolt, J. F.; Fanconi, B. *Macromolecules* **1978**, *11*, 740−745.

(49) Hsu, S. L.; Reynolds, N.; Bohan, S. P.; Strauss, H. L.; Snyder, R. G. *Macromolecules* **1990**, *23*, 4565−4575.

(50) Kobayashi, M.; Sakashita, M.; Adachi, M.; Kobayashi, M. *Macromolecules* **1995**, *28*, 316−324.

(51) Schwarz, R.; Seelig, J.; Künnecke, B. *Magn. Reson. Chem.* **2004**, *42*, 512−517.

(52) Borodin, O.; Smith, G. D.; Bedrov, D. *J. Phys. Chem. B* **2002**, *106*, 9912−9922.

(53) Albinsson, B.; Michl, J. *J. Phys. Chem.* **1996**, *100*, 3418−3429.

(54) Schwickert, H.; Strobl, G.; Kimmig, M. *J. Chem. Phys.* **1991**, *95*, 2800−2806.

(55) Albrecht, T.; Elben, H.; Jaeger, R.; Kimmig, M.; Steiner, R.; Strobl, G.; Stühn, B.; Schwickert, H.; Ritter, C. *J. Chem. Phys.* **1991**, *95*, 2807−2816.

(56) Albrecht, T.; Jaeger, R.; Petry, W.; Steiner, R.; Strobl, G.; Stühn, B. *J. Chem. Phys.* **1991**, *95*, 2817−2822.

(57) Rysanek, N.; Coquillay, M.; Bourgaux, C.; Ollivon, M. *J. Phys. Chem. B* **2002**, *106*, 11870−11875.

(58) Uyar, T.; Hunt, M. A.; Gracz, H. S.; Tonelli, A. E. *Cryst. Growth Des.* **2006**, *6*, 1113−1119.

(59) Levitt, M. H. *In Spin Dynamics*; John Wiley & Sons Ltd.: Chichester, 2001.

(60) Lyerla, J. R., Jr.; VanderHart, D. L. *J. Am. Chem. Soc.* **1976**, *98*, 1697−1700.